# *FUSE* observations of the Blue Compact Dwarf Galaxy Mrk 59[1]

Trinh X. Thuan

*Astronomy Department, University of Virginia, Charlottesville, VA 22903*

txt@virginia.edu

Alain Lecavelier des Etangs

*Institut d'Astrophysique de Paris, CNRS, 98 bis bld Arago, F-75014 Paris, France*

lecaveli@iap.fr

and

Yuri I. Izotov

*Main Astronomical Observatory, National Academy of Sciences of Ukraine, 03680, Kyiv, Ukraine*

izotov@mao.kiev.ua

## ABSTRACT

New *FUSE* far-UV spectroscopy of the nearby metal-deficient ($Z_\odot/8$) cometary Blue Compact Dwarf (BCD) galaxy Markarian (Mrk) 59 is discussed. The data are used to investigate element abundances in its interstellar medium. The H I absorption lines are characterized by narrow cores which are interstellar in origin and by broad wings which are stellar in origin. The mean interstellar H I column density is $\sim 7 \times 10^{20}$ cm$^{-2}$ in Mrk 59. No $H_2$ lines are seen and $N(H_2)$ is $\lesssim 10^{15}$ cm$^{-2}$ at the 10 $\sigma$ level. The lack of diffuse $H_2$ is due to the combined effect of a strong UV radiation field which destroys the $H_2$ molecules and a low metallicity which leads to a scarcity of dust grains necessary for $H_2$ formation. P-Cygni profiles of the S VI 933.4, 944.5 Å and O VI 1031.9, 1037.6 Å lines are seen, indicating the presence of very hot O stars and a stellar wind terminal velocity of $\sim 1000$ km s$^{-1}$. By fitting the line profiles with multiple components having each a velocity dispersion $b = 7$ km s$^{-1}$ and spanning a radial velocity range of 100 km s$^{-1}$, some of which can be saturated, we derive heavy element abundances in the neutral gas. We find log $N$(O I)/$N$(H I) = –5.0±0.3 or [O I/H I] = –1.5 for the neutral gas, about a factor of 10 below the oxygen abundance of the supergiant H II region, implying self-enrichment of the latter.

*Subject headings:* galaxies: individual (Mrk 59) — galaxies: dwarf — galaxies: compact — ultraviolet: galaxies — galaxies: abundances — galaxies: ISM — ISM: molecules — galaxies: starburst

## 1. Introduction

The Blue Compact Dwarf (BCD) galaxy Markarian 59 (Mrk 59) ≡ I Zw 49 belongs to the class of cometary BCDs defined by Loose & Thuan (1985) as characterized by an intense starburst at the end of an elongated low surface brightness (LSB) stellar body. In the case of Mrk 59, the elongated body is named NGC 4861. Arp (1966) describes NGC 4861 in his Atlas of Peculiar Galaxies as "an object with irregular clumps, resolved into knots with a very bright knot (diameter = 1 kpc) at the southeastern end". The knots are in fact a chain of H II regions, resulting probably from propagating star formation along the galaxy's elongated body and ending with the high-surface-brightness supergiant H II region at the southeastern end (Noeske et al. 2000). Dinerstein & Shields (1986) first detected broad Wolf-Rayet stellar features in Mrk 59 indicating the presence of late nitrogen and early carbon Wolf-Rayet stars. Guseva, Izotov & Thuan (2000) using the spectroscopic observations of Izotov, Thuan & Lipovetsky (1997) found that several dozens of Wolf-Rayet stars are present. Noeske et al. (2000) used deep ground-based spectrophotometric observations of the supergiant H II region to derive an Oxygen abundance log O/H = –4.011 ± 0.003 ($Z_{\odot}/8$), typical of BCDs. O abundances were also derived for two other emission knots along the elongated body and were found to be the same within the errors. The small scatter in metallicity along the major axis of Mrk 59 ($\sim$ 0.2 dex) suggests that the mixing of elements in the ionized gas has been efficient on a spatial scale of several kpc. Wilcots, Lehman & Miller (1996) and Thuan, Lévrier & Hibbard (2001) have used the VLA to map NGC 4861 and Mrk 59 in the 21 cm line. With a beam size of 15″ (780 pc), the latter authors found a very clumpy interstellar medium (ISM) with H I column densities ranging from a few $10^{19}$ to a few $10^{21}$ cm$^{-2}$. Despite irregularities, the H I velocity field of NGC 4861 resembles that of a rotating disk seen almost edge-on. Spectral population synthesis in combination with color-magnitude diagrams and color profiles give a most probable age of $\sim$ 2 Gyr for the LSB elongated body, with an upper limit of $\sim$ 4 Gyr (Noeske et al. 2000), considerably smaller than the typical age (5 Gyr or greater) of the underlying stellar population in BCDs of other types, and making Mrk 59 a relatively young galaxy.

---

[1]Based on observations made with the NASA-CNES-CSA *Far Ultraviolet Spectroscopic Explorer*. *FUSE* is operated for NASA by the Johns Hopkins University under NASA contract NAS5-32985.

Because of these interesting properties and its brightness in the far-ultraviolet (Kinney et al. (1993) list an *IUE* $\lambda$1432 – 1532 Å flux of $\sim 10^{-13}$ erg s$^{-1}$ cm$^{-2}$ Å$^{-1}$), Mrk 59 is a prime target in our *Far Ultraviolet Spectroscopic Explorer (FUSE)* studies of BCDs. In particular, we wish to study the molecular hydrogen content and heavy element abundances in its interstellar medium (ISM). Thuan et al. (2001) obtained a H I heliocentric velocity of 847 km s$^{-1}$. Using the Virgocentric infall model of Schechter (1980) with parameters $\gamma = 2$, $v$(Virgo) = 976 km s$^{-1}$, $w_\odot = 220$ km s$^{-1}$ and $D$(Virgo) = 15.9 Mpc, then the distance of Mrk 59 is 10.7 Mpc. At this distance, 1″ corresponds to 52 pc. Mrk 59 has $m_B = 12.64$ (Noeske et al. 2000), so that $M_B = -17.51$.

We describe the *FUSE* observations in section 2. In section 3, we derive the Hydrogen column density by fitting the profiles of the H I Lyman series lines. In section 4, we set upper limits on the amount of diffuse $H_2$. In section 5, we derive the interstellar ionic abundances by fitting the profiles of the metallic absorption lines with multiple components, and compare the heavy element abundances in the neutral and ionized gas. In section 6, we discuss the O VI and S VI stellar lines with their P-Cygni profiles, and derive a terminal stellar wind velocity. We summarize our findings in section 7.

## 2. Observations

Mrk 59 ($\alpha_{2000} = 12^h59^m00\overset{s}{.}3$, $\delta_{2000} = 34°50'42\overset{''}{.}8$; $l^{II} = 111\overset{\circ}{.}54$, $b^{II} = 82\overset{\circ}{.}12$) was observed during 7,865 s on 2000, January 11 with *FUSE* (Moos et al. 2000). The LWRS large entrance aperture (30″× 30″) was used, so that all of Mrk 59 which is $\sim 20''$ across (Noeske et al. 2000) is included within it. Flux was recorded in both long wavelength (LiF, $\sim$ 1000 – 1187 Å) and both short wavelength (SiC, $\sim$ 900 – 1100 Å) channels. The pipeline version 1.5 has been used to process the data. The spectral resolution is defined by both the instrument and the size of the galaxy. We find it to be about 10,000 with a signal-to-noise ratio (S/N) of $\sim$ 10 per resolution element. This a relatively high S/N for this type of object as observed by *FUSE* (compare for example the spectrum of Mrk 59 in Figure 1 with that of the BCD I Zw 18 obtained by Vidal-Madjar et al. 2000).

The *FUSE* spectrum shows two absorption line systems at two different radial velocities: one system of $H_2$ lines is at –250 km s$^{-1}$ and the other is at 600 km s$^{-1}$. Since the $H_2$ lines arise in the Milky Way, there is a systematic wavelength shift of –250 km s$^{-1}$ over the whole spectrum. Taking into account that shift, the other absorption line system corresponds to a velocity of 850 km s$^{-1}$ which matches well the H I heliocentric velocity of 847 km s$^{-1}$ of Mrk 59 (Thuan et al. 2001). A wavelength blueshift of 100 km s$^{-1}$ has also been seen in the *FUSE* spectrum of the BCD I Zw 18 by Vidal-Madjar et al. (2000). This systematic

wavelength shift is probably due to the preliminary wavelength calibration of *FUSE* and a slight offset of the target from the center of the slit.

Figure 1 shows the entire *FUSE* spectrum shifted to the rest-frame of Mrk 59. We have marked the most prominent interstellar absorption lines: the H I Lyman series and absorption lines from other atoms and ions such as C II, C III, N I, N II, N III, O I, Si II, S III, S IV, Fe II and Fe III. Several stellar features such as the Si IV and S VI lines have been also detected and are marked by dotted lines. There are no evident emission features except for the blue emission in the P-Cygni profiles of the stellar O VI and S VI lines. We have also marked the rest wavelengths of the interstellar absorption lines arising in the Galaxy at the bottom of each panel in Figure 1.

## 3. Narrow cores and broad wings of the H I Lyman series line profiles: interstellar and stellar absorption

The relatively high S/N of the *FUSE* spectrum of Mrk 59 gives us an unique opportunity to study the absorption lines from the nearly entire Lyman series of Hydrogen from Ly $\beta$ to Ly $\lambda$ (H I 11), except for Ly $\alpha$ which is out of the wavelength range covered by *FUSE*. The foreground Galactic H I column density in the direction of Mrk 59 is $2.8 \times 10^{20}$ cm$^{-2}$ (Heiles 1975). Adopting a smooth continuum, we have used Voigt profiles to fit the observed H I Lyman series lines. The fitting routine used was a modified version of the Owens profile fitting procedure developed by Martin Lemoine and the *FUSE* French team. This program returns the most likely values of many free parameters like the Doppler widths and column densities by a $\chi^2$ minimization of the difference between the observed and computed profiles. The latest version of this program is particularly suited to the characteristics of *FUSE* spectra. For example, it allows for a variation of the background level, a double gaussian point spread function, and a shift of the wavelength scale. These are taken as free parameters which are dependent on the wavelength region and determined by the $\chi^2$ minimization. A special version has been developed to fit the absorption lines in the particular case of galaxies where the observed spectrum is the sum of the fluxes coming from thousands of stars through different absorbers with varying column densities.

We found, to our surprise, that the shapes of the H I Lyman series lines cannot be reproduced with profiles characterized by a single H I column density. Figure 2 illustrates the problem. The upper-left panel shows the Lyman $\zeta$ line. Damping wings are clearly visible, signaling a very large H I column density $N($ H I$) \sim 5 \times 10^{22}$ cm$^{-2}$. The fit corresponding to that column density is shown by the lower dashed line. However, this high column density is not consistent with the shape of the other H I lines. For example, the upper-right panel shows

the H I Lyman $\delta$ line. Although damping wings are also present, the core of the Lyman $\delta$ line is thin and cannot be fitted with a model profile with the column density needed to fit the Lyman $\zeta$ line (lower dashed line), the predicted core being too wide. The thin core implies a smaller column density, of the order of $10^{21}$ cm$^{-2}$ (upper dashed line), the expected value for a line of sight going through the ISM of the whole galaxy. Thus the problem is the following: assuming that the H I Lyman series absorption lines are of interstellar origin, then at least two types of H I column densities are needed, one type with $N$ (H I) $\sim 10^{21}$ cm$^{-2}$ and the other with $N$ (H I) $\sim 5 \times 10^{22}$ cm$^{-2}$. A bimodal distribution of $N$ (H I) is also needed in the fitting of the Lyman $\beta$ line shown in the bottom panel of Figure 2. We can only fit its red wing as the blue wing is contaminated by the Earth's airglow. The dashed lines show respectively, from bottom to top, model profiles for H I column densities of $5 \times 10^{22}$, $10^{22}$, $3 \times 10^{21}$, and $10^{21}$ cm$^{-2}$. None of these profiles is able to fit the observed shape of the line. Again, a very large H I column density of the order of $10^{23}$ cm$^{-2}$ is needed to explain the broad damping wings, whereas its core is very narrow requiring a column density of the order of $10^{21}$ cm$^{-2}$.

A first interpretation of the bimodality of $N$(H I) is that the absorbing interstellar medium in front of the far-UV-bright stars is very inhomogeneous. Since the observed spectrum is the sum of spectra of individual stars located behind H I clouds with different column densities, and there are more than $10^3$ lines of sight to stars emitting in the far-UV over the $\sim 20''$ wide central region of Mrk 59, these may go through H I clouds with widely different column densities. To test that hypothesis in a more rigorous manner, we have performed a fit of the H I Lyman series lines by considering various mixtures of 23 different H I column densities which span nearly 3 orders of magnitude, from a few $10^{20}$ to $10^{23}$ cm$^{-2}$. The resulting fit is found by $\chi^2$ minimization of the difference between the computed and observed profiles of the H I lines, from Lyman $\beta$ to Lyman $\eta$, when varying the fractions of the contributing column densities. That fit is shown by solid lines for the Ly $\beta$, Ly $\delta$ and Ly $\zeta$ lines in Figure 2. The corresponding H I column density distribution is shown in Figure 3. As expected from the consideration of individual lines, the $N$ (H I) distribution is bimodal, with one peak near $5 \times 10^{20}$ cm$^{-2}$ and the other near $10^{23}$ cm$^{-2}$. As discussed before, the high H I column densities are required to fit the damping wings of the H I lines further up in the Lyman series, particularly from the Ly $\delta$ to the Ly $\lambda$ lines. On the other hand, the core of the Lyman lines further down the series are considerably narrower. For example, the Lyman $\beta$ line has a core width of less than 1 Å, corresponding to a column density below $10^{21}$ cm$^{-2}$. About 1/3 of the Mrk 59 far-UV flux is seen through H I clouds with a "normal" column density while about 2/3 of the flux is absorbed by H I with very high column densities.

There are several problems with attributing the very high $N$(H I) to interstellar clouds.

First, H I interstellar column densities as high as $10^{23}$ cm$^{-2}$ are not seen. The highest known H I column density known thus far in a BCD is $7 \times 10^{21}$ cm$^{-2}$ in SBS 0335–052 (Thuan & Izotov 1997). With a cloud of column density $\sim 10^{23}$ cm$^{-2}$ covering the whole galaxy, the core of the Lyman $\beta$ line would have been several Å wide, which is not observed. Second, if the high column density is due to an interstellar cloud covering about $\sim 2/3$ of the area of Mrk 59, the associated dust would strongly absorb the far-UV photons, which is not the case.

We thus need to find other explanations for the broad damping wings responsible for the high derived column densities. One source of line broadening is wavelength smearing effects due to the extended nature of the source. However, we do not believe those to be the main cause of the broad H I wings because of several reasons. First, they fall far short from accounting for the very large widths of the damping wings. Indeed the size of the *FUSE* aperture (30 arcsec) and the size of the observed galaxy (less than 20 arcsec) give a wavelength smearing of $\pm$30 km s$^{-1}$. This is significanty below the half width at half-maximum of the Fe III line which is larger than 100 km s$^{-1}$, and more than one order of magnitude lower than the half-widths of the wings of the H I lines, observed to be $\sim$ 1000 km s$^{-1}$ for the Ly$\delta$ and Ly$\gamma$ lines, and above 4000 km s$^{-1}$ for the Ly$\beta$ line. Second, many other lines are very narrow. For instance, the Galactic $H_2$ absorption lines have full widths at half-maximum (FWHM) less than 30 km s$^{-1}$. If the broad wings are due solely to wavelength smearing, then all lines should show them, not just hydrogen lines. Third, the hydrogen lines in the *FUSE* spectrum of the BCD I Zw 18 which is comparable in angular size ($\sim 20''$) and was obtained through the same aperture (Vidal-Madjar et al. 2000) do not show the broad wings seen in Mrk 59. Hence, the latter cannot be attributed to instrumental effects. While wavelength smearing effects due to the extended nature of the source may indeed give a measured velocity dispersion $b$ larger than the true value, they cannot be mainly responsible for the broad wings of the H I lines.

Given that the broad wings of the higher order Lyman lines are not caused by instrumental effects, what physical effect may be responsible for them? The possibility that they are due to H I cloud motions is unlikely because the lines have symmetric profiles and their large widths correspond to velocities of several hundred to more than a thousand km s$^{-1}$. Such high velocities are not evident either in the single-dish H I profile of Mrk 59 (Thuan & Martin 1981) or in its H I VLA map (Thuan et al. 2001). A more plausible explanation is that the wide damping wings are not interstellar in origin, but stellar. Many of the broad absorption features in the *FUSE* spectrum of Mrk 59 (Fig. 1) such as the S VI 933.4, 944.5 Å, O VI 1031.9, 1037.6 Å lines with P Cygni profiles, the broad Si IV 1128.3 Å, N IV 955.3 Å and blue-shifted C III 1175.7 Å lines are undoubtedly formed in atmospheres of massive stars with spectral types ranging from the earliest O to early B types. Some other broad

lines such as the H I Lyman series lines discussed before, the C III 977.0 Å, N III 989.8 Å, S III 1012.4 Å and Fe III 1122.5 Å lines can be formed both in the interstellar medium and in the atmospheres of stars. Examination of far-UV spectra of early B stars in the effective temperature range 20000 – 25000 K based on Kurucz (1991)'s models does indeed reveal hydrogen and ion lines with considerable wings. H I Lyman lines with broad wings are also seen in *FUSE* spectra of B stars (Fremat et al. 2001). Thus we conclude that the broad wings of the above lines in Mrk 59 arise in the photospheres of the numerous B stars in the BCD, while their narrower cores are caused by interstellar absorption.

We point out however that, besides the B stars, there is also a population of more massive early O stars in Mrk 59. This is evidenced by the detection of the S VI 1031.9, 1037.6 Å and O VI 1031.9, 1037.6 Å lines in the *FUSE* spectrum (section 6). These lines are only present in the most massive stars. Additional support for the presence of a population of early O stars comes from the optical spectrum of Mrk 59 (e.g., Izotov et al. 1997; Guseva et al. 2000) where strong emission lines are present. The equivalent width ($EW$) of the H$\beta$ emission line of $\sim$ 150 Å puts strong constraints on the age of the starburst. In the case of an instantaneous burst model, the observed $EW$(H$\beta$) gives a burst age of only $\sim$ 4 Myr, approximately the lifetime of a 60 $M_\odot$ star (Schaerer & Vacca 1998). In the case of continuous star formation, the observed $EW$(H$\beta$) can be reproduced by a stellar population constantly forming between 0.1 and 10 Myr. In this case, massive stars should also be present. Finally, evidence for the presence of very massive stars in Mrk 59 comes from the detection of broad Wolf-Rayet features at 4650 Å and 5808 Å. According to Schaerer & Vacca (1998), at the metallicity of Mrk 59, Wolf-Rayet stars are descendants of main-sequence stars with masses greater than 40 – 50 $M_\odot$.

Thus, while stars from early O to early B types are responsible for the continuum distribution and its slow intensity decrease for wavelengths shorter than 950 Å, the broad wings of the H I Lyman series lines and some heavy element lines originate in the photospheres of early B stars. We note that the wings of the H I Ly$\beta$ line are not as broad in the BCD I Zw 18 so that both core and wings can be fitted with a single interstellar H I column density (Vidal-Madjar et al. 2000). This can be due to I Zw 18 having a younger stellar population with predominantly hot O stars in its star-forming region. However, only the Ly$\beta$ line has been fitted in I Zw 18, half the *FUSE* wavelength range being not available in the Vidal-Madjar et al.' spectrum. This may not be enough to reveal the problem.

By fitting the cores of the Lyman series lines, we obtain an interstellar H I column density in Mrk 59 of $N$(H I) $\sim 7 \times 10^{20}$ cm$^{-2}$. $N$(H I) is estimated as the weighted mean of all column densities contributing to the first peak in the bimodal distribution of Figure 3, i.e all those with a value less than $10^{22}$ cm$^{-2}$.

## 4. Upper limits on the diffuse $H_2$ content of Mrk 59

$H_2$ lines from the Milky Way are detected up to levels of at least J = 3 in the spectrum of Mrk 59, with column densities of a few $10^{20}$ cm$^{-2}$ (Fig. 1). However, no line of $H_2$ is seen at the radial velocity of the BCD despite the fact that Mrk 59 has H I column densities very similar to those in the Milky Way.

From a VLA H I map of Mrk 59 (Thuan et al. 2001), we derive a velocity dispersion $b = 20$ km s$^{-1}$ which we use to calculate upper limits to the $H_2$ column densities. Using Voigt profiles for the $H_2$ lines, we construct a series of synthesized spectra with varying $H_2$ column densities, compute the difference between each synthesized spectrum and the observed spectrum in nine Lyman bands (0–0 to 8–0), and calculate the increase in the $\chi^2$ of the fit to the observed spectrum. The upper limits given in Table 1 for the $N(H_2)$ column densities in Mrk 59 correspond to an increase of $\chi^2$ by a factor of 100, meaning that they are 10 $\sigma$ limits. Because most of the $H_2$ molecules are in the J = 0 or J = 1 levels at temperatures typical of the interstellar medium, we conclude that the total column density of $H_2$ is $\lesssim 10^{15}$ cm$^{-2}$. Fig. 4 shows the expected $H_2$ lines if the column density of $H_2$ had been $10^{15}$ cm$^{-2}$ for the J = 0, 1 and 2 levels. It is clear that $H_2$ with such a column density in Mrk 59 would have been easily detected by *FUSE*. With a H I column density of $\sim 7 \times 10^{20}$ cm$^{-2}$, this implies that the ratio of $H_2$ to H I is $\lesssim 10^{-6}$ in the absorbing clouds in front of Mrk 59. The corresponding average molecular fraction $f = 2N(H_2)/(N(H\ I)+2N(H_2))$ is $\lesssim 3 \times 10^{-6}$. Adopting a diameter of 1 kpc for Mrk 59 gives an upper limit of $\sim 12\ M_\odot$ for the total mass of diffuse $H_2$.

This is a very stringent upper limit. Only one BCD, I Zw 18, has been searched previously by *FUSE* for diffuse $H_2$ (Vidal-Madjar et al. 2000). These authors also established an upper limit for the diffuse $H_2$ column density of $\sim 10^{15}$ cm$^{-2}$, corresponding to $M(H_2) \lesssim 30\ M_\odot$. Thus our $H_2$ upper limits for Mrk 59 confirm and strengthen the results of Vidal-Madjar et al. Of course, these limits concern only diffuse $H_2$ along the line of sights to the several thousands of far-UV bright massive stars in Mrk 59. Our *FUSE* observations are not sensitive to clumpy $H_2$ in very compact star-forming regions. High dust extinction in these regions would prevent the far-UV photons of the massive young stars from escaping. The dust distribution being clumpy, the far-UV photons go out preferentially along lines of sight that are devoid of dust. This is deduced from the observation that the extinction derived from UV spectra is significantly smaller than the value derived from the Balmer decrement as measured from the optical spectra of the same object. The UV light preferentially emerges through windows of low optical depth (Fanelli, O'Connell & Thuan 1988). This implies that, in some regions, the dust is efficiently destroyed or removed from the vicinity of young massive O stars by the combined action of ionizing radiation, stellar winds, and supernovae.

Since dust is needed for efficient formation of $H_2$ molecules, its absence along particular lines of sight implies that these molecules will also be absent along those directions.

Two possible formation mechanisms of $H_2$ without dust grains have been proposed. The first mechanism is via the formation of the negative ion $H^-$ ($H + e \rightarrow H^- + e$), followed by the associative reaction $H^- + H \rightarrow H_2 + e$, where the electrons come from the photoionization of carbon (Jenkins & Peimbert 1997). The second mechanism consists of the radiative association of H and $H^+$ to form $H_2^+$, which then results in $H_2$ by the capture of an electron. However these two mechanisms are extremely inefficient under the temperatures ($10^2$ – $10^4$ K) and densities ($10^2$ – $10^4$ cm$^{-3}$) prevailing in the ISM of Mrk 59 and will not be discussed further. We shall thus only consider the case where $H_2$ is formed on the surface of grains.

In that case, to detect $H_2$ molecules, we need to probe dusty regions. Near-infrared (NIR) and mid-infrared (MIR) observations serve well that purpose since infrared photons suffer less extinction from dust and can escape more easily than UV photons. Indeed, $H_2$ emission lines are seen in the NIR emission-line spectra of some of these objects (Vanzi & Rieke 1997 and Vanzi et al. 2000). Most spectacular is the case of the BCD SBS 0335–052 ($Z_\odot/41$), the second most metal-deficient BCD known after I Zw 18 ($Z_\odot/50$). Thuan, Sauvage & Madden (1999) derived from *ISO* $\lambda$5–17 $\mu$m observations an extinction $A_V \sim$ 20 mag for SBS 0335–052. Such a large extinction implies that a significant fraction (as much as $\sim$ 75%) of the current star formation activity in SBS 0335–052 is hidden by dust whose total mass is $\sim$ 3000 $M_\odot$. Optical photons cannot get out of these very compact star-forming regions, much less UV photons. There is some evidence that the strengths of the $H_2$ emission lines are correlated with the amount of dust present in these objects. Thus the line intensity ratio of the (1,0)S(1) $H_2$ line to the Br$\gamma$ H I line in SBS 0335–052 is among the highest observed for BCDs.

To summarize, $H_2$ molecules are probably present in Mrk 59, but their distribution is clumpy and most likely follows that of the dust. *FUSE* does not see this $H_2$ because it selects out line of sights going through regions devoid of dust.

We now check whether the absence of diffuse $H_2$ is reasonable, given the physical conditions in the H I cloud surrounding Mrk 59. These conditions must be quite different from those in the Milky Way since Mrk 59 has H I column densities similar to those seen in the Milky Way for which diffuse $H_2$ is strongly detected while it is conspicuously absent in the BCD (Fig. 4). We first explore the situation at the edge of the cloud. From the VLA map of Thuan et al. (2001), the angular radius of the H I cloud is 180″ or $R_0 = 9.4$ kpc. From the *FUSE* spectra, the radiation flux at 1000 Å at Earth is $\sim 2.3 \times 10^{-13}$ erg s$^{-1}$ cm$^{-2}$ Å$^{-1}$. Correcting for the Galactic extinction $E(B-V) = 0.011$ mag (Schlegel, Finkbeiner & Davis 1998) with $A(1000\ \text{Å}) = 5.742\ A_V = 0.2$ mag (Cardelli, Clayton & Mathis 1989) gives a flux

at $R_0$ from the ionizing stars $F_{R_0} = 3.6 \times 10^{-7}$ erg s$^{-1}$ cm$^{-2}$ Å$^{-1}$. We have assumed the internal extinction in the far-UV to be negligible, as argued before. By solving the grain temperature equilibrium equation obtained by equating the radiation absorbed by grains to that emitted, and adopting the approximations by Vidal-Madjar et al. (2000), we obtain a grain temperature at the edge of the H I cloud of 11 $(a/0.1\ \mu\mathrm{m})^{-1/6}$ K, where $a$ is the radius of the grain assumed to be spherical. The grain temperature increases as $R^{-1/3}$ closer to Mrk 59, and at the edge of the star-forming region at a radius of 10″ or $R_0 = 0.52$ kpc, it is 29 $(a/0.1\ \mu\mathrm{m})^{-1/6}$ K. We conclude that the range of grain temperatures in the H I cloud around Mrk 59 is very similar to that in the diffuse interstellar medium of the Milky Way, and that $H_2$ formation can indeed occur.

To calculate the amount of $H_2$ molecules formed on the surface of dust grains, we assume that the $H_2$ formation rate scales with metallicity, i.e. that its value in Mrk 59 is 1/8 the Galactic value since the metallicity of Mrk 59 is 1/8 that of the Sun. Following the assumptions described by Vidal-Madjar et al. (2000), at equilibrium, when the formation of $H_2$ on dust equals its destruction rate by UV photons, the molecular fraction $f(H_2) = 2n(H_2)\ /\ [2n(H_2) + n(H)]$ (where $n(H_2)$ and $n(H)$ denote the number densities of $H_2$ and H) in Mrk 59 is proportional to $Z_{\mathrm{Mrk\,59}} n(H)/I$, where $I$ is the flux of $H_2$ dissociating photons. We can write $f(H_2)$ as:

$$f(H_2) = 1.6 \times 10^{-34} \left(\frac{Z_{\mathrm{Mrk\,59}}}{Z_\odot}\right) \left(\frac{F_{R_0}}{\mathrm{erg\,s^{-1}cm^{-1}\AA^{-1}}}\right)^{-1} \left(\frac{R_0}{\mathrm{kpc}}\right)^{-1} \left(\frac{N(\mathrm{HI})}{\mathrm{cm^{-2}}}\right).$$

With the approprate numerical values for Mrk 59, we find $f(H_2) \sim 6 \times 10^{-30}\ N(\mathrm{H\ I})$. Thus the $H_2$ column density $N(H_2)$ is $\sim 3 \times 10^{-30}\ N(\mathrm{H\ I})^2$. For $N(\mathrm{H\ I})$ equal to $7 \times 10^{20}$ cm$^{-2}$, the expected $N(H_2)$ is $\sim 2 \times 10^{12}$ cm$^{-2}$, nearly three orders of magnitude below and consistent with our established upper limit. As compared to the Milky Way, the low column density of diffuse $H_2$ in Mrk 59 is due to the combined effects of a large UV flux which destroys the $H_2$ molecules and of a low metallicity resulting in a scarcity of dust grains on which to form them.

## 5. Heavy element abundances

We next derive heavy element abundances by fitting the profiles of the metal absorption lines. The line profile fitting method is superior to a simple curve-of-growth analysis because it allows to simultaneously fit the lines from different heavy elements in Mrk 59 and also the $H_2$ lines in the Milky Way. This permits in turn to constrain in a self-consistent manner several parameters such as the $b$ parameter, the instrumental profile and the background

level. A curve-of-growth method does not allow easily for such an analysis.

In performing the line profile fitting, we have considered two cases. The first case is probably less realistic, but gives lower limits to the abundances in the interstellar medium of Mrk 59. It assumes that there is a single velocity component along the line of sight to the BCD. Consequently, lines that are broader than the point spread function and do not go down to zero intensity level are supposed to be not saturated. The second case considers multiple velocity components along the line of sight, some of which may have saturated profiles. It is probably closer to the true situation.

### 5.1. Profile fitting with a single velocity component

We consider first the single interstellar velocity component case. Several absorption lines of neutral and singly, doubly and triply ionized ions of heavy elements are detected in the *FUSE* spectrum of Mrk 59. The most prominent ones are the C II 1036.3 Å, C III 977 Å, N I 1135.0 Å, N II 1084.0 Å, O I 1039.2 Å, S III 1012.5 Å, S IV 1062.7 Å, Fe II 1144.9 Å and Fe III 1122.5 Å lines. They are are marked in Figure 1 by solid lines. Some of the lines, for example the Fe III 1122.5 Å and S III 1012.5 Å lines, are very broad. A single Voigt interstellar profile fit to these lines would give unreasonably large Doppler widths, $b \gtrsim 100$ km s$^{-1}$ (Table 2). The large widths suggest, as in the case of the H I Lyman series lines, that these metal lines are not only interstellar in origin but also have some contamination by stellar absorption. Indeed, we found that the profiles of these broad lines can be well fitted by using the bimodal distribution of column densities found for neutral hydrogen $N$(H I) and shown in Figure 3, and by varying only a single parameter, the ratio of the species's column density to that of H I, $N$(element)/$N$(H I).

For example, the fit to the S III 1012.5 Å line profile based on the $N$(H I) distribution in Fig. 3 is shown by a thick line in Fig. 5. No good fit can be obtained with a single ion column density and a reasonably low $b$ parameter, for example 42 km s$^{-1}$, as shown by the dashed lines in Fig. 5 for $N$(S III) equal to $8 \times 10^{14}$ and $4 \times 10^{15}$ cm$^{-2}$. As in the case for the Lyman series H I lines, none of these dashed profiles can account simultaneously for both the width and the depth of the observed line, the width of the line requiring high column densities, while its shallowness requiring low column densities. The ratio which gives the best fit to the S III line profile is $N$(S III)/$N$(H I) $= 8 \times 10^{-8}$. For the lines of other species like O I 1039.2 Å and N I 1135.0 Å, good fits can be obtained with Voigt profiles with $b$ values between 20 and 40 km s$^{-1}$. The resulting column densities and Doppler widths $b$ along with their error bars are given in Table 2 under the heading log $N_1$(species) for the most prominent interstellar absorption lines. The error bars of the column densities include

the uncertainty in $b$. Only a lower limit to the column density is given for the C II 1036.3 Å line. It is derived not from profile fitting, but from the equivalent width of the line as only its blue wing can be observed, its red wing being contaminated by Earth's airglow. A fit to the blue wing alone would give a considerably larger value: $N(\mathrm{C\ II}) \gg 10^{17}$ cm$^{-2}$.

Taken at face value, the abundances of the metals relative to $N$(H I) are extremely low as compared to the solar values. In particular, with log $N(\mathrm{O\ I})/N(\mathrm{H\ I}) = -5.7$ and using the Meyer et al. (1998)' value for the Galactic ISM, we obtain [O I/H I] = –2.2. Thus, if the O I line has its origin in the neutral gas, the oxygen abundance in the H I gas is $\sim 50$ times lower than the oxygen abundance in the ionized gas, as determined from the optical emission line spectrum of the supergiant H II region in Mrk 59. It is $\sim 7$ times lower than the oxygen abundance in the star-forming region of I Zw 18, the most metal-deficient BCD known. However, these very low abundances may be caused by the saturation of some lines, which we discuss next.

### 5.2. Profile fitting with multiple velocity components

If there is a single velocity component along the line of sight, then the fact that the lines, for instance the O I and Fe II lines, do not go to zero intensity although they are broader than the instrumental point spread function determined with the $H_2$ lines of the Milky Way, would argue for them not to be saturated. However, because Mrk 59 is extended, we are observing the BCD along thousands of lines of sight through the *FUSE* aperture, so the observed spectrum is the sum of many narrower spectra with different velocities. It can happen that some lines of sight have saturated absorption lines with a small $b$ parameter, but because they have different radial velocities spread over several tens of km s$^{-1}$, the broad absorption line resulting from the sum of many narrow absorption lines does not go to zero intensity, and its width is larger than the point spread function. In that case, a single velocity component fit to the line profile would result in an overestimate of the $b$ parameter and in an underestimate of the column density.

To investigate this issue, we have calculated profiles resulting from the addition of multiple lines of sight for all heavy element lines with good enough S/N. We adopt the simple model where the different lines of sight have radial velocities distributed uniformly between $v_{\mathrm{Mrk59}} - \Delta v/2$ and $v_{\mathrm{Mrk59}} + \Delta v/2$, where $v_{\mathrm{Mrk59}}$ is the radial velocity of Mrk 59 and $\Delta v$ is the spread in velocity due mostly to the velocity dispersion of the system of absorbing clouds along the multiple lines of sight, and also partly to the wavelength smearing caused by the extension of Mrk 59 within the aperture. We determine the best fit to several lines of O I, N I and Fe II simultaneously by varying $b$ (assumed to be the same for all lines

of sight) and $\Delta v$, so as to minimize the $\chi^2$ of the difference between the observed and computed profiles. Because the spectrum of Mrk 59 shows several lines of the same element with different oscillator strengths, the $b$ and $\Delta v$ parameters, which are independent of the chemical element considered, can be constrained reasonably well.

The best solution was obtained for $b = 7^{+13}_{-3}$ km s$^{-1}$ and $\Delta v = 100\pm20$ km s$^{-1}$, where the error bars are $2\sigma$ limits. These values are physically quite reasonable. The $b$ value is similar to those found for individual absorbing clouds in the ISM of the Milky Way. As for the value of $\Delta v$, it is very close to the FWHM of 92 km s$^{-1}$ of the H I profile (Thuan et al. 2001). However the $30''$ *FUSE* aperture does not sample all the neutral gas which extends over some $6'$ in diameter. Thus the observed velocity spread $\Delta v$ is probably due to the combined effect of rotational and random motion of the absorbing cloud system, plus some wavelength smearing because of the extension of the source. Figure 6 shows the fits to the O I 1039 Å absorption line and to the N I 1134 Å multiplet. The best fit is shown by the thick solid line. It is evident that the multi-component fit is much better than the single-component fit (thin line in Figure 6b). Figure 6a also shows an example of a narrow component along one light of sight which has a saturated profile (dotted line).

The heavy element column densities derived with the multi-component fit, along with their $2\sigma$ error bars are given in Table 2 under the heading log $N_2$(species). As expected, the derived abundances are larger than in the case of a single component fit, by a mean factor of $\sim 5$. The very large column densities derived for C III, S III and Fe III are caused by stellar contamination as discussed before. We obtain log $N$(O I)/$N$(H I) = –5.0±0.3 or [O I/H I] = –1.5. It is highly probable that [O/H] $\sim$ [O I/H I] as the ionization potentials of Hydrogen and Oxygen are very close to each other. Moreover, the charge exchange cross-section of O II with H I is large, making it unlikely that Oxygen is more ionized than Hydrogen. This appears to be supported by the remarkable constancy of [O I/H I] in the local ISM of the Galaxy, independently of direction and ionizing flux (Meyer et al. 1998), in strong contrast to [N I/H I] which depends on the ionizing conditions. Given that [O/H] = –5.0, the H I absorbing cloud has a metallicity lower than that of the supergiant H II region by a factor of $\sim 10$. This suggests self-contamination of the H II region by heavy elements released during the present burst of star formation (Kunth & Sargent 1986). While mixing of these newly formed heavy elements appears to have occurred on a scale of $\sim$ 2 kpc as shown by the small scatter of the average metallicities of the H II regions in the vicinity of the supergiant H II region (Noeske et al. 2000), it has not had time to occur for the whole neutral gas component as the H I envelope surrounding the star-forming regions is much more extended (its diameter is $\sim$ 19 kpc from the VLA map by Thuan et al. 2001).

### 5.3. Modeling

We attempt next to model the observed heavy element column densities. The presence of the higher ionization stages of these elements implies that the ions reside not exclusively in the H I envelope, but also in the H II regions around the ionizing stars. We use the CLOUDY code (Ferland 1996, Ferland et al. 1998; version c90.05) to construct a series of photoionized H II region models, and select the one which best reproduces the optical nebular emission line intensities observed in Mrk 59 (Izotov et al. 1997). By comparing the predicted column densities of the best photoionization model with those observed by *FUSE*, we will be able to tell which fraction of metals resides in the neutral gas and which fraction is in the ionized gas.

We consider a spherically symmetric ionization-bounded H II region model. The calculations are stopped in the zone away from the ionizing stars where the temperature drops to 2000 K. The ionization in this zone is very low and it is taken to be the outer edge of the H II region. Several input parameters need to be set. First, the distance to Mrk 59 is taken to be 10.7 Mpc. For this distance and using the aperture-corrected H$\beta$ flux from Guseva et al. (2000), we derive an H$\beta$ luminosity $L(\mathrm{H}\beta) = 1.15 \times 10^{40}$ erg s$^{-1}$, and a number of ionizing photons $N(\mathrm{Lyc}) = 2.45 \times 10^{52}$ s$^{-1}$. We use the Kurucz (1991) stellar atmosphere models and adopt the effective temperature of the ionizing stellar radiation to be $T_{\mathrm{eff}} = 50{,}000$ K, a typical value for low-metallicity high-excitation H II regions. For the inner radius of the H II region, we adopt $R_{\mathrm{in}} = 10^{19}$ cm. The chemical composition of the H II region is set by the observed element abundances derived from optical spectroscopy of Mrk 59 (Izotov & Thuan 1999), except for the carbon abundance. For carbon we adopt log C/O = –0.4 which is intermediate between the solar value and that for the lowest-metallicity BCDs (Izotov & Thuan 1999). The adopted abundances are shown in Table 3.

We run the CLOUDY code varying the filling factor $f$ and the electron number density in order to obtain the best agreement between the predicted and observed [O II] and [O III] emission lines. The best model is found for a filling factor $f = 0.1$ and an electron number density $N_{\mathrm{e}} = 25$ cm$^{-3}$. The optical line intensities of the best model are shown in Table 4, where we compare them with the observed ones (Izotov et al. 1997). There is good general agreement, giving us confidence that the photoionization model is correct. The predicted total hydrogen (neutral and ionized) column density in the H II region is $N(\mathrm{H\ I} + \mathrm{H\ II}) = 1.88 \times 10^{21}$ cm$^{-2}$ or log $N(\mathrm{H\ I} + \mathrm{H\ II}) = 21.27$. As expected for a H II region model, most of the hydrogen is ionized: $N(\mathrm{H\ II}) = 1.86 \times 10^{21}$ cm$^{-2}$. The column density of the neutral hydrogen is two orders of magnitude lower. The model also predicts a column density of molecular hydrogen made via $\mathrm{H}^-$ $N(\mathrm{H}_2) = 5.78 \times 10^{11}$ cm$^{-2}$, more than 3 orders of magnitude lower than our observational upper limit.

We now compare the predictions for the column densities of heavy elements with those derived from the *FUSE* spectrum in the more realistic case of multiple velocity component fitting (column 5 of Table 2). The CLOUDY predictions are shown in Table 5. The ones relevant to the *FUSE* observations are also given in column 6 of Table 2. In Table 5, $x$ is the radially averaged ratio of the ion number to the total number of a particular element, e.g., $N(\mathrm{Fe}^{+})/N(\mathrm{Fe})$. The predicted log $N$(X) of species X is then derived as log $N$(X) = log $N$(H I+H II) + log $\mathrm{X}^{+i}/\mathrm{H}$ – log $x(\mathrm{X}^{+i})$. Comparison of columns 5 and 6 in Table 2 reveals that for all lines that do not suffer from stellar contamination, the derived column densities are larger than the CLOUDY predictions by a mean factor of $\sim 5$ (a factor of 2.5 for O I), except for the S IV ion which has a column density smaller than the predicted one, but consistent with it within the errors. Thus it is clear that there has been previous metal enrichment of the neutral ISM of Mrk 59. While the neutral gas is less metal-rich than the ionized gas by a factor 10 (section 5.2), the neutral gas column densities are larger by a factor of $\sim 5$ because of the larger extent of the neutral as compared to the ionized gas.

## 6. The O VI and S VI stellar lines and their P-Cygni profiles

Several stellar emission and absorption lines are also seen in the spectrum of Mrk 59. They are marked in Figure 1 by dotted lines. The S VI 933.4, 944.5 Å, O VI 1031.9, 1037.6 Å lines show redshifted emission associated with blueshifted absorption, characteristic of stellar lines with P Cygni profiles. Such broad P Cygni lines are known to originate in stellar winds of O stars, and have been detected in several environments during previous space missions: in the Galaxy by *Copernicus* (Snow & Jenkins 1977; Morton 1976, 1979; Morton & Underhill 1977; Walborn & Bohlin 1996) and in the Magellanic Clouds during the *HUT/Astro2* mission (Walborn et al. 1995). More recently, studies of O stars with stellar winds have been undertaken with *FUSE* (Bianchi et al. 2000; Fullerton et al. 2000). Although the O VI and S VI stellar lines with P Cygni profiles have been seen in O stars of all spectral and luminosity subtypes, they are most prominent and show the strongest redshifted emission in the hottest and most luminous stars: for example, in the O4f star $\zeta$ Pup in the Galaxy (Morton 1976; Morton & Underhill 1977) and in some O3 – O4 stars in the Large and Small Magellanic Clouds (Walborn et al. 1995). Morton (1976) estimated the mass of $\zeta$ Pup to be $\sim 100\ M_{\odot}$. The presence of the O VI and S VI P Cygni profiles in the *FUSE* spectrum of Mrk 59 thus implies the presence of such very massive O stars in the BCD. The spectrum does not have, however, the necessary signal-to-noise ratio to allow us to carry out a detailed quantitative analysis of the properties of those stars with stellar winds.

Additionally, a broad blueshifted C III 1175.7 Å stellar absorption line is seen in the spectrum of Mrk 59, with very little redshifted emission. This type of P-Cygni profile associated with the C III line is prominent in the spectra of O and early B supergiants (e.g., Walborn & Bohlin 1996). Unlike the O VI and S VI lines, the C III line is relatively free of contamination by other absorption lines, and its width allows us to estimate the velocity of the stellar wind associated with the massive stars in Mrk 59. The width as measured from the rest wavelength to the wavelength of the most blueshifted point of the profile is $\sim 4$ Å, which corresponds to a terminal stellar wind velocity of $\sim 1000$ km s$^{-1}$. This value is slightly smaller than the terminal velocities of $\sim 1400$ km s$^{-1}$ found for O stars in the Small Magellanic Cloud (e.g., Bianchi et al. 2000), which has a metallicity comparable to Mrk 59. That terminal velocity is on the other hand considerably lower than typical wind velocities observed for O stars in the Galaxy. For example, Morton (1979) derived a terminal velocity of 2660 km s$^{-1}$ for $\zeta$ Pup. However, the terminal stellar wind velocity in Mrk 59 is larger than the velocity of $\sim 500$ km s$^{-1}$ found by Thuan & Izotov (1997) in SBS 0335–052 which has a much lower metallicity (1/41 solar). There appears to be a general trend of smaller terminal velocities with decreasing metallicities. This trend can be understood since less metals means less opacity to drive stellar winds and hence lower velocities.

It is very likely that the width of the blueshifted absorption in the O VI P-Cygni profiles is similar to that in the C III line. The expected broad absorption of the two O VI 1031.9, 1037.6 Å lines would then be superimposed on the red wing of the Ly$\beta$ line, causing a broad depression in that part of its profile. Figure 1 shows indeed that the profile of the Ly$\beta$ line is distinctly asymmetric, with the red wing being generally at a lower flux level than the blue wing. We note that this asymmetry of the Ly$\beta$ line is also present in the *FUSE* spectrum of other starburst galaxies such as NGC 1705 (Heckman et al. 2001).

There is no evidence for a velocity shift between the absorption lines arising from the gas and the stellar features, so that there is no outflow motion from the starburst region.

## 7. Summary

We present new *FUSE* far-UV spectroscopy of the metal-deficient ($Z_\odot/8$) cometary Blue Compact Dwarf (BCD) galaxy Markarian 59 (Mrk 59). We have obtained the following results:

1. The very high signal-to-noise of the *FUSE* spectrum allows us to study the absorption lines from the nearly entire Lyman series of Hydrogen from Ly $\beta$ to Ly $\lambda$ (H I 11). The H I lines are characterized by narrow cores and broad damping wings, requiring a bimodal

distribution of H I column densities to fit their profiles, with one set of column densities with values of a few times $10^{20}$ cm$^{-2}$ and the other with values of $\sim 10^{23}$ cm$^{-2}$. This bimodality can be understood if the cores of the H I absorption lines are interstellar in origin while the broad damping wings are produced by stellar absorption. By fitting the cores of the Lyman series lines, we obtain a mean interstellar H I column density in Mrk 59 of $\sim 7 \times 10^{20}$ cm$^{-2}$.

2. No $H_2$ lines are detected in Mrk 59. We set a 10 $\sigma$ upper limit for the total column density of diffuse $H_2$ of $10^{15}$ cm$^{-2}$. This low $H_2$ column density, as compared to the one in the Milky Way which has a similar H I column density, is due to the combined effects of a large UV flux which destroys $H_2$ molecules and of a low metallicity resulting in a scarcity of dust grains on which to form the molecules. This limit does not exclude the possible presence of clumpy $H_2$ in dusty compact star-forming regions from which the far-UV photons cannot escape, and which *FUSE* cannot see.

3. Many interstellar absorption lines of neutral and singly, doubly and triply ionized ions of heavy elements are detected in the *FUSE* spectrum of Mrk 59. The most prominent ones are the N I 1135.0 Å, N II 1084.0 Å, O I 1039.2 Å, S III 1012.5 Å, S IV 1062.7 Å and Fe II 1144.9 Å lines. We have derived element abundances by modeling the profiles of detected absorption lines as the sum of multiple profiles with velocity dispersion $b = 7$ km s$^{-1}$ and radial velocity spanning a range of 100 km s$^{-1}$, some of which can be saturated. We find $\log N(\text{O I})/N(\text{H I}) = -5.0 \pm 0.3$ or [O I/H I] = –1.5 for the neutral gas, about a factor of 10 below the oxygen abundance of the supergiant H II region, and implying self-enrichment of the latter.

4. We have used the CLOUDY code to construct a photoionized H II region model which best reproduces the optical emission line intensities in the supergiant H II region. The derived column densities for heavy elements in the neutral gas are about 5 times higher than those predicted by CLOUDY for the ionized gas, implying previous metal enrichment of the H I gas. Although the neutral gas is a factor of 10 more metal-deficient than the ionized gas, its heavy element column densities are 5 times higher because of the considerably larger extent of the H I envelope as compared to the supergiant H II region.

5. The S VI 933.4, 944.5 Å and O VI 1031.9, 1037.6 Å lines with P-Cygni profiles are seen, originating in stellar winds of hot O stars. The terminal stellar wind velocity is $\sim$ 1000 km s$^{-1}$ as compared to $\sim$ 2500 km s$^{-1}$ in the Milky Way, suggesting a trend of smaller terminal velocities with decreasing metallicities.

The profile fitting was done using the Owens procedure developed by M. Lemoine and the *FUSE* French Team. T.X.T. thanks the financial support of NASA grant NAG5-8954. He acknowledges the hospitality of the Institut d'Astrophysique de Paris and the Departement

d'Astronomie extragalactique et de Cosmologie at the Observatoire de Meudon during his sabbatical year. T.X.T. and Y.I.I. are grateful for the partial financial support of NSF grant AST-96-16863. Y.I.I. thanks the hospitality of the Astronomy Department of the University of Virginia.

## REFERENCES

Arp, H. C. 1966, ApJS, 14, 1

Bianchi, L., et al. 2000, ApJ, 538, l57

Cardelli, J. A., Clayton, G. C., & Mathis, J. S. 1989, ApJ, 345, 245

Dinerstein, H. L., & Shields, G. A. 1986, ApJ, 311, 45

Fanelli, M. N., O'Connell, R. W., & Thuan, T.X. 1988, ApJ, 334, 665

Ferland, G. J. 1996, CLOUDY, Univ. of Kentucky, Dept. of Phys. and Astron. Internal Rep.

Ferland, G. J., Korista, K. T., Verner, D. A., Ferguson, J. W., Kingdon, J. B., & Verner, E. M. 1998, PASP, 110, 761

Fremat, Y. et al. 2001, A&A, submitted

Fullerton, A. W., et al. 2000, ApJ, 538, L43

Guseva, N. G., Izotov, Y. I., & Thuan, T. X. 2000, ApJ, 531, 776

Heckman, T. M., Sembach, K. R., Meurer, G. R., Strickland, D. K., Martin, C. L., Calzetti, D., & Leitherer, C. 2001, ApJ, in press

Heiles, C. 1975, A&AS, 20, 37

Izotov, Y. I., & Thuan, T. X. 1998, ApJ, 500, 188

———. 1999, ApJ, 511, 639

Izotov, Y. I., Thuan, T. X., & Lipovetsky, V. A. 1997, ApJS, 108, 1

Jenkins, E. B., & Peimbert, A. 1997, ApJ, 477, 265

Kinney, A. L., Bohlin, R. C., Calzetti, D., Panagia, N., & Wyse, R. F. G. 1993, ApJS, 86, 5

Kunth, D. & Sargent, W.L.W. 1986, ApJ, 300, 496

Kurucz, R. L. 1991, in Stellar Atmospheres: Beyond Classical Models, NATO ASI series C, Vol. 341, eds. L. Crivellari, I. Hubeny & D. G. Hummer, 441

Loose, H.-H., & Thuan, T. X. 1985, in Star-forming Dwarf Galaxies and Related Objects, ed. D. Kunth, T. X. Thuan & J. T. T. Van (Gif-sur-Yvette: Editions Frontières), 73

Meyer, D. M., Jura, M., & Cardelli, J. A. 1998, ApJ, 493, 222

Moos, H.W., et al. 2000, ApJ, 538, L1

Morton, D. C. 1976, ApJ, 203, 386

———. 1979, MNRAS, 189, 57

Morton, D. C., & Underhill, A. B. 1977, ApJS, 33, 83

Noeske, K. G., Guseva, N. G., Fricke, K. J., Izotov, Y. I., Papaderos, P., & Thuan, T. X. 2000, A&A, 361, 33

Schechter, P. L. 1980, AJ, 85, 801

Schlegel, D. J., Finkbeiner, D. P., & Davis, M. 1998, ApJ, 500, 525

Snow, T. P., & Jenkins, E. B. 1977, ApJS, 33, 269

Thuan, T. X., & Izotov, Y. I. 1997, ApJ, 489, 623

Thuan, T. X., Lévrier, F., & Hibbard, J. E. 2001, in preparation

Thuan, T. X., & Martin, G. M. 1981, ApJ, 247, 823

Thuan, T. X., Sauvage, M., & Madden, S. 1999, ApJ, 516, 783

Vanzi, L., Hunt, L. K., Thuan, T. X., & Izotov, Y. I. 2000, A&A, 363, 493

Vanzi, L., & Rieke, G. H. 1997, ApJ, 479, 694

Vidal-Madjar, A. et al. 2000, ApJ, 538, L77

Walborn, N. R., & Bohlin, R. C. 1996, PASP, 108, 477

Walborn, N. R., Long, K. S., Lennon, D. J., & Kudritzki, R.-P. 1995, ApJ, 454, L27

Wilcots, E. M., Lehman, C., & Miller, B. 1996, AJ, 111, 1575

Table 1. Upper limits on the $H_2$ content of Mrk 59 at the $\sim 10\ \sigma$ level

| Molecule | J | $N(H_2)$ ($cm^{-2}$) |
|---|---|---|
| $H_2$ | 0 | $< 2 \times 10^{14}$ |
| | 1 | $< 5 \times 10^{14}$ |
| | 2 | $< 4 \times 10^{14}$ |
| | 3 | $< 3 \times 10^{14}$ |
| | 4 | $< 3 \times 10^{14}$ |
| | 5 | $< 4 \times 10^{14}$ |

Table 2. Heavy element column densities ($cm^{-2}$) in Mrk 59

| Species | $\lambda$(Å) | $b_1$ (km $s^{-1}$)[a] | log $N_1$(species) [a] | log $N_2$(species) [b] | CLOUDY |
|---|---|---|---|---|---|
| C II | 1036.3 | ··· | >14.6 | ··· | 15.5 |
| C III | 977.0 | $\leq 35$ | $18.4^{+0.1}_{-0.1}$ | $18.2^{+0.1}_{-0.1}$ | 16.8 |
| N I | 1135.0 | 40±20 | $14.0^{+0.3}_{-0.4}$ | $14.6^{+0.4}_{-0.3}$ | 13.7 |
| N II | 1084.0 | 30±10 | $14.2^{+0.1}_{-0.2}$ | $15.1^{+2.2}_{-0.8}$ | 14.4 |
| O I | 1039.2 | 40±20 | $15.1^{+0.3}_{-0.3}$ | $15.8^{+0.3}_{-0.3}$ | 15.4 |
| S III | 1012.4 | 95±15 | $15.1^{+0.1}_{-0.1}$ | $19.0^{+0.1}_{-0.2}$ | 15.4 |
| S IV | 1062.7 | 30±10 | $14.2^{+0.1}_{-0.2}$ | $14.9^{+0.9}_{-0.6}$ | 15.3 |
| Fe II | 1144.9 | 40±15 | $13.9^{+0.1}_{-0.2}$ | $14.4^{+0.3}_{-0.3}$ | 13.7 |
| Fe III | 1122.5 | 105±10 | $15.1^{+0.1}_{-0.1}$ | $18.9^{+0.1}_{-0.1}$ | 14.1 |

[a]Fitting with a single Voigt profile. Error bars are 3 $\sigma$ limits.

[b]Fitting with multiple velocity components, each with $b_2 = 7$ km $s^{-1}$, and spanning a velocity range of 100 km $s^{-1}$. Error bars are 2 $\sigma$ limits. The C III 977.0 Å, S III 1012.4 Å and Fe III 1122.5 Å lines have high column densities because of stellar contamination.

Table 3. Abundances in Mrk 59 used as input to CLOUDY[a]

| Species | $N$(species)/$N$(H) |
|---|---|
| He[b] | −1.08 |
| C | −4.41 |
| N | −5.53 |
| O | −4.01 |
| Ne | −4.75 |
| Si | −5.35 |
| S | −5.55 |
| Ar | −6.34 |
| Fe | −5.92 |

[a]From Izotov & Thuan (1999).

[b]Corresponding to a He mass fraction $Y = 0.248$ (Izotov & Thuan 1998).

Table 4. Comparison between the observed and CLOUDY predicted optical line intensities normalized to H$\beta$

| Ion | Observed[a] | CLOUDY |
|---|---|---|
| 3727 [O II] | 1.102 | 1.035 |
| 3835 H9 | 0.086 | 0.081 |
| 3868 [Ne III] | 0.449 | 0.502 |
| 3889 He I + H8 | 0.201 | 0.196 |
| 3968 [Ne III] + H7 | 0.311 | 0.317 |
| 4068 [S II] | 0.010 | 0.012 |
| 4101 H$\delta$ | 0.265 | 0.266 |
| 4340 H$\gamma$ | 0.468 | 0.476 |
| 4363 [O III] | 0.089 | 0.082 |
| 4471 He I | 0.036 | 0.040 |
| 4658 [Fe III] | 0.005 | 0.004 |
| 4740 [Ar IV] | 0.006 | 0.006 |
| 4861 H$\beta$ | 1.000 | 1.000 |
| 4959 [O III] | 1.982 | 1.992 |
| 5007 [O III] | 5.802 | 5.750 |
| 5271 [Fe III] | 0.002 | 0.002 |
| 5876 He I | 0.106 | 0.109 |
| 6300 [O I] | 0.019 | 0.010 |
| 6312 [S III] | 0.017 | 0.019 |
| 6363 [O I] | 0.006 | 0.003 |
| 6563 H$\alpha$ | 2.819 | 2.833 |
| 6584 [N II] | 0.046 | 0.031 |
| 6678 He I | 0.030 | 0.031 |
| 6717 [S II] | 0.095 | 0.074 |
| 6731 [S II] | 0.071 | 0.053 |
| 7065 He I | 0.025 | 0.024 |
| 7136 [Ar III] | 0.076 | 0.076 |
| 7320 [O II] | 0.016 | 0.015 |
| 7330 [O II] | 0.014 | 0.013 |

[a]From Izotov et al. (1997).

Table 5. CLOUDY predicted column densities

| Ion | log $x^{a}$ | log $N^{b}$ |
|---|---|---|
| C II | −1.354 | 15.51 |
| C III | −0.098 | 16.77 |
| C IV | −0.800 | 16.06 |
| N I | −2.023 | 13.72 |
| N II | −1.367 | 14.38 |
| N III | −0.104 | 15.64 |
| O I | −1.876 | 15.39 |
| O II | −1.224 | 16.04 |
| O III | −0.033 | 17.23 |
| Si II | −1.256 | 14.67 |
| Si III | −0.324 | 15.60 |
| Si IV | −0.580 | 15.34 |
| S II | −1.463 | 14.26 |
| S III | −0.289 | 15.44 |
| S IV | −0.393 | 15.33 |
| Ar I | −2.220 | 12.71 |
| Fe II | −1.677 | 13.68 |
| Fe III | −1.277 | 14.08 |
| Fe IV | −0.034 | 15.32 |

[a]Radially averaged ratio of the ion number to the total number of the element.

[b]Column density in $cm^{-2}$.

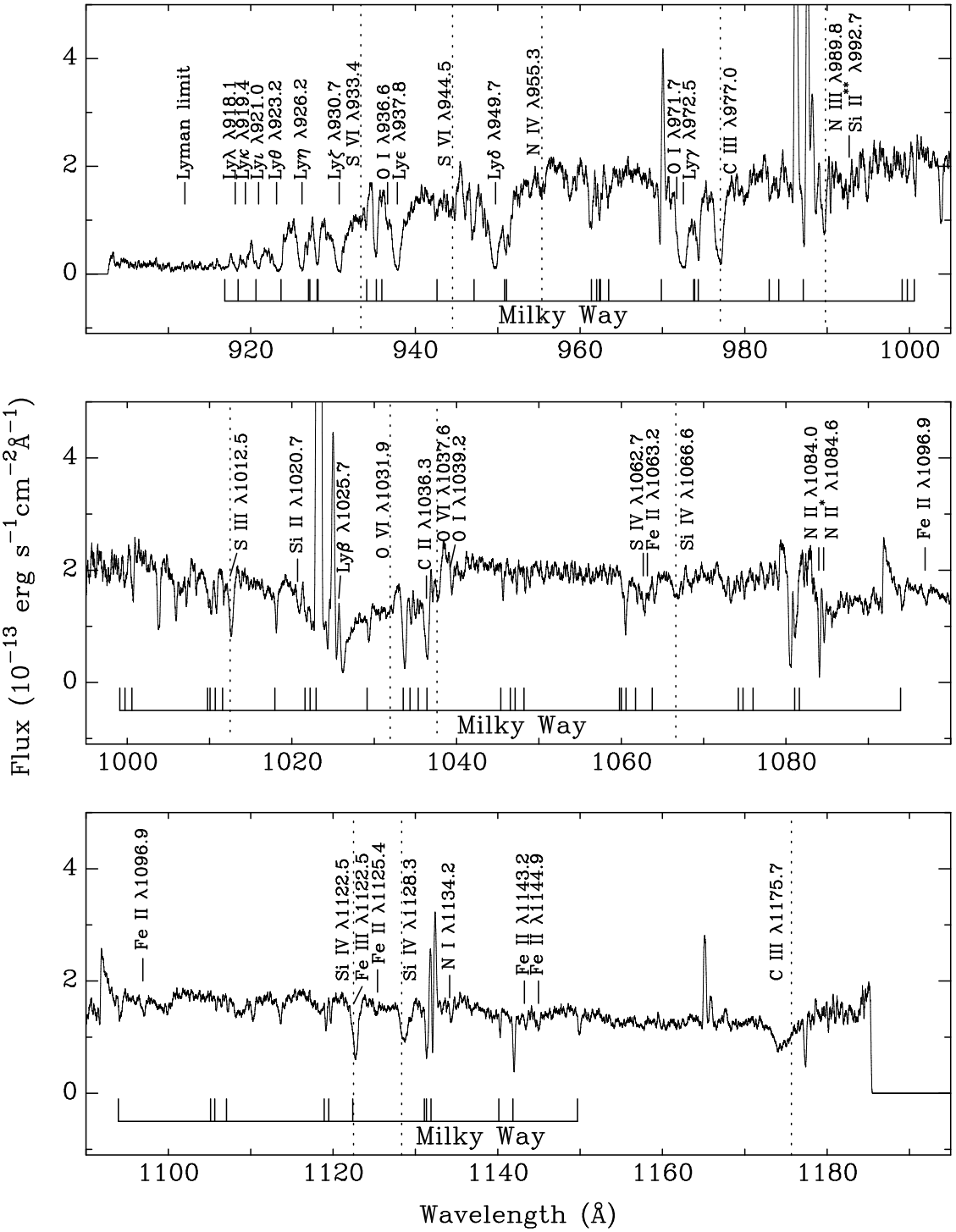


Fig. 1.— Rest-frame *FUSE* spectrum of Mrk 59. The data has been smoothed by a 11-point box-car. Prominent interstellar absorption lines are indicated. The lines arising in Mrk 59 are marked on top and those in the Milky Way at bottom. Particularly prominent in Mrk 59 are the H I Lyman series lines. There are also strong interstellar absorption lines from the C II, C III, N I, N II, O I, S III, S IV, Fe II and Fe III lines. The rest wavelenghts of the stellar lines in Mrk 59 are shown by dotted lines. The S VI, O VI and C III λ1175.7 lines show P-Cygni profiles.

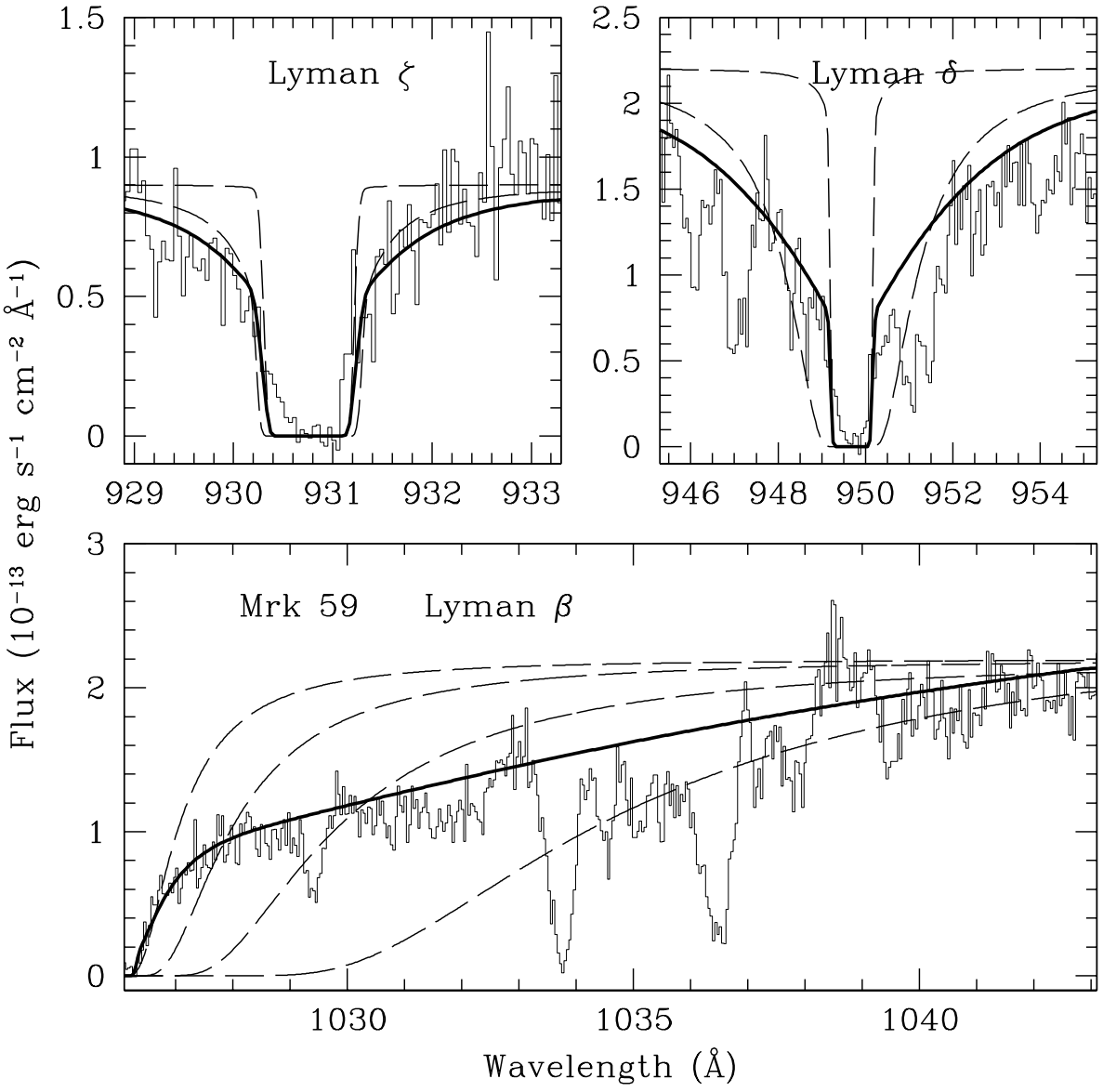


Fig. 2.— Profile fitting of 3 H I Lyman series lines. The solid lines show the best fit, with the distribution of H I column densities shown in Fig. 3. The dashed lines show fits with a single column density of respectively $10^{21}$ and $5 \times 10^{22}$ cm$^{-2}$ in the case of the Lyman $\zeta$ and $\delta$ lines and $10^{21}$, $3 \times 10^{21}$, $10^{22}$ and $5 \times 10^{22}$ cm$^{-2}$ in the case of the red wing of the Lyman $\beta$ line. It is evident that a single column density does not provide a good fit to the entire profile. We argue that the cores of the lines are interstellar in origin while the broad wings are stellar in origin.

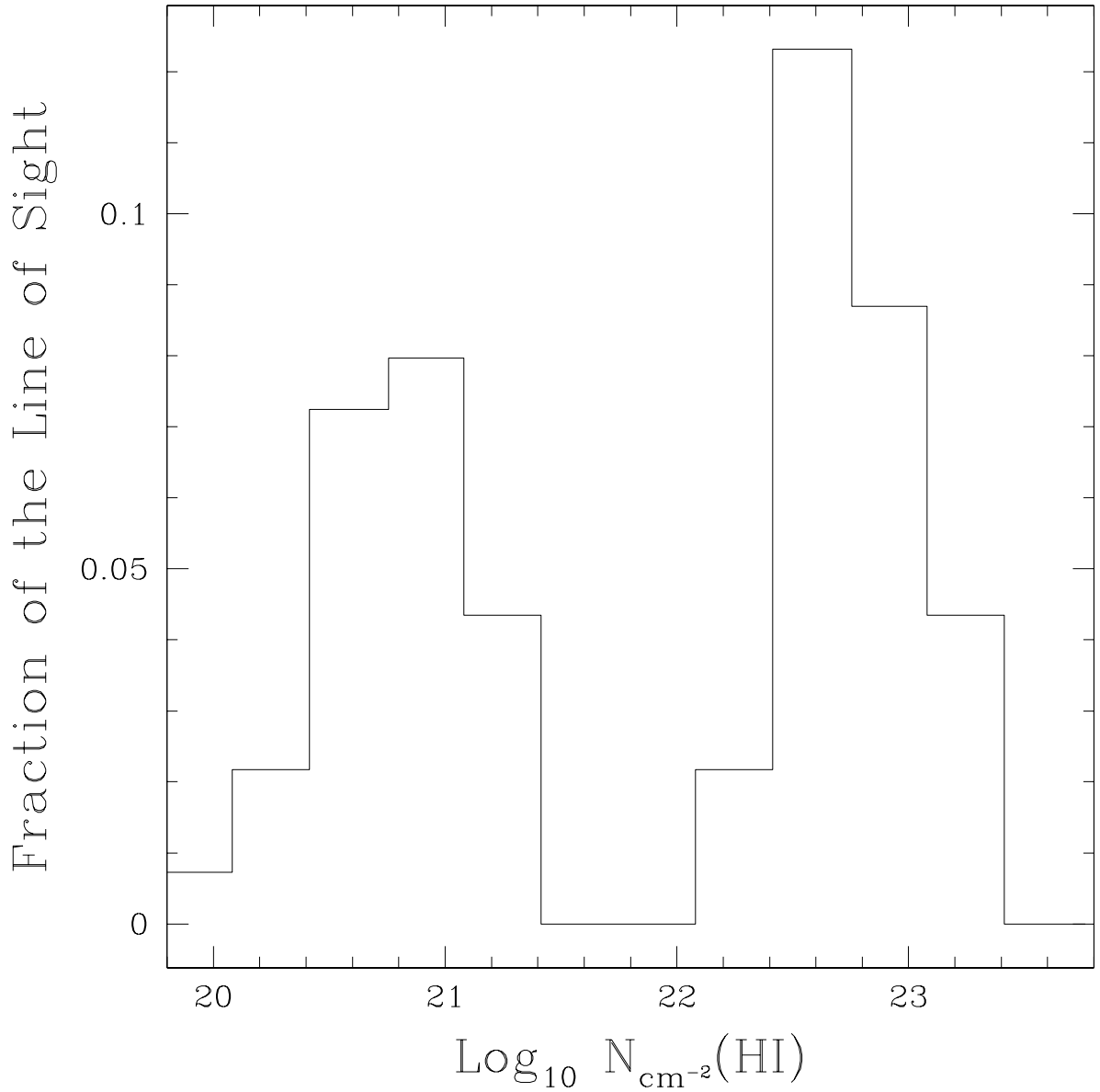


Fig. 3.— Distribution of H I column densities needed to fit the absorption profiles of some H I Lyman series lines (see Fig. 2). The distribution is bimodal: $\sim \frac{1}{3}$ of the lines of sight to the far-UV bright sources have a H I column density of a few $10^{20}$ cm$^{-2}$, while $\sim \frac{2}{3}$ have a H I column density of $\sim 10^{23}$ cm$^{-2}$. We argue that the first peak is due to interstellar clouds while the second peak is due to stellar photospheres.

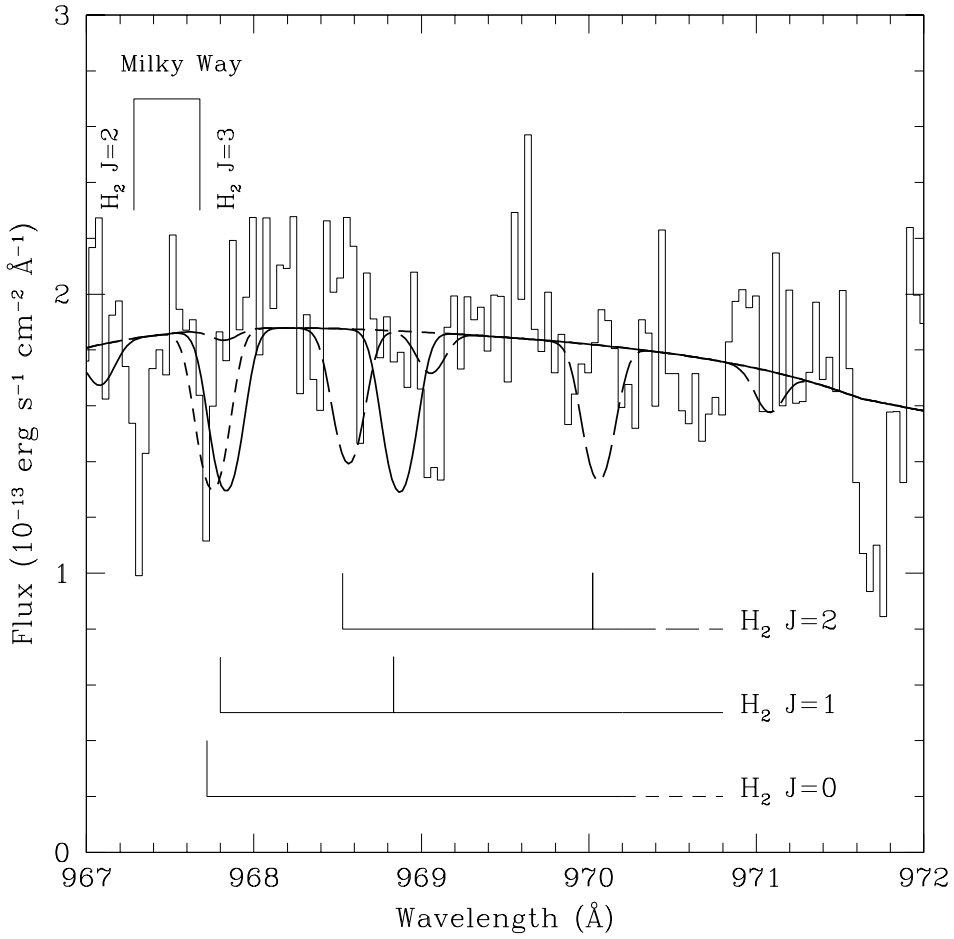


Fig. 4.— Plot of the expected $H_2$ lines from the Werner series (0-2) if $H_2$ were present in Mrk 59 at the 10 $\sigma$ level. Molecular hydrogen lines from the Milky Way which has a H I column density comparable to Mrk 59 are easily detected and marked here for the J = 2 and J = 3 levels. The spectral region shown is only one out of a total of 18 regions in the spectrum used to constrain the upper limit of $H_2$. The $H_2$ line profiles corresponding to a $H_2$ column density of $10^{15}$ cm$^{-2}$ are shown for the J = 0 (long-dashed line), J = 1 (solid line) and J = 2 (short-dashed line) levels.

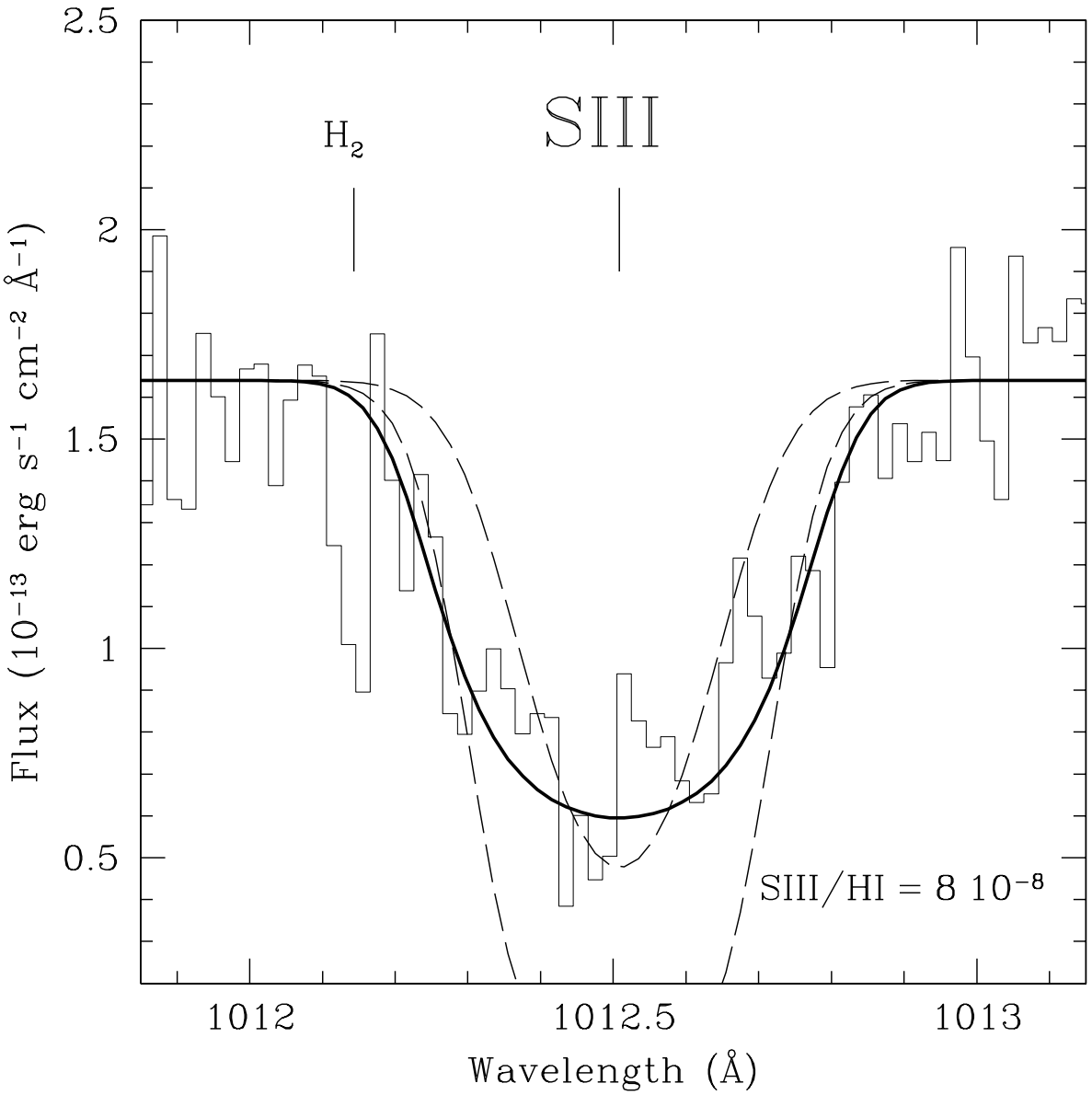


Fig. 5.— Profile fitting of the absorption line of ion S III. The solid line shows the best fit obtained using the H I column density distribution shown in Figure 3 and varying the ratio of $N$(ion)/$N$(H I). The ratio corresponding to the best fit is $8 \times 10^{-8}$. The dashed lines show Voigt profile fitting with $b = 42$ km s$^{-1}$ and S III column densities equal respectively to $8 \times 10^{14}$ (upper line) and $4 \times 10^{15}$ cm$^{-2}$ (lower line).

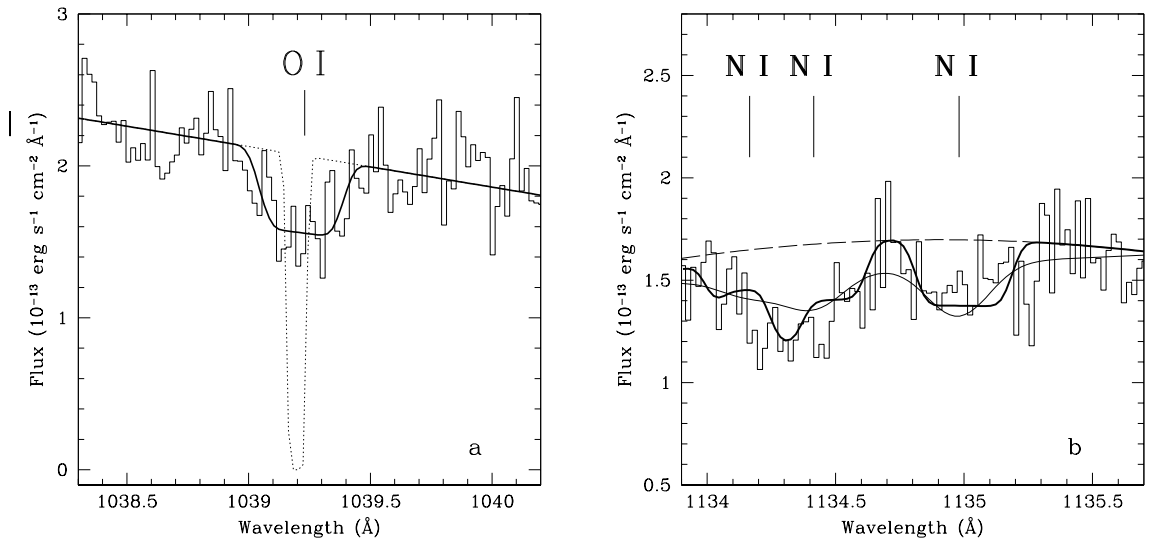


Fig. 6.— a) Fit to the O I 1039Å absorption line with a column density $N(\mathrm{O\ I}) = 7 \times 10^{15}\mathrm{cm}^{-2}$. The fit is obtained by the addition of multiple profiles with radial velocities uniformly distributed between $v_{\mathrm{Mrk59}} - \Delta v/2$ and $v_{\mathrm{Mrk59}} + \Delta v/2$. $\Delta v$ and the $b$ parameter are constrained by the simultaneous fit of several lines of O I, N I and Fe II. The thick solid line gives the resulting fit to the data with $\Delta v = 100$ km s$^{-1}$ and $b = 7$ km s$^{-1}$. The dotted line represents an example of one line of sight with $b = 7$ km s$^{-1}$. With this column density, such an individual line of sight is saturated and goes down to the zero intensity level. However the absorption line observed by *FUSE* resulting from the addition of many narrower profiles does not go to the zero intensity level, although it is broader than the width of the instrumental point spread function ($\sim 0.1$Å). b) Fit to the N I 1134Å multiplet with a N I column density $N(\mathrm{N\ I}) = 4 \times 10^{14}$ cm$^{-2}$. The thick solid line gives the multi-component fit to the data with $\Delta v = 100$ km s$^{-1}$ and $b = 7$ km s$^{-1}$. The thin solid line gives the best fit obtained with a simple Voigt profile, with $N(\mathrm{N\ I}) = 10^{14}$ cm$^{-2}$ and $b = 40$ km s$^{-1}$. It is clear that the multi-component fit is better than the single component fit. In the former case, the line at 1135Å is saturated and fainter than the two other lines at 1134.2Å and 1134.4Å.